Received: 14 November 2023 | Revised: 29 December 2023 | Accepted: 4 January 2024

DOI: 10.1002/pro.4903

RESEARCH ARTICLE

THE PROTEIN SOCIETY WILEY

Exploring the dynamics and structure of PpiB in living *Escherichia coli* cells using electron paramagnetic resonance spectroscopy

Yasmin Ben-Ishay[1] | **Yoav Barak**[2] | **Akiva Feintuch**[1] | **Olivier Ouari**[3] | **Annalisa Pierro**[4] | **Elisabetta Mileo**[4] | **Xun-Cheng Su**[5] | **Daniella Goldfarb**[1]

[1]Department of Chemical and Biological Physics, Weizmann Institute of Science, Rehovot, Israel

[2]Department of Chemical Research Support, Weizmann Institute of Science, Rehovot, Israel

[3]CNRS, ICR, Institut de Chimie Radicalaire, Aix-Marseille Université, Marseille, France

[4]CNRS, BIP, Laboratoire de Bioénergétique et Ingénierie des Protéines, Aix Marseille Université, Marseille, France

[5]State Key Laboratory of Elemento-organic Chemistry, Tianjin Key Laboratory of Biosensing and Molecular Recognition, College of Chemistry, Nankai University, Tianjin, China

Correspondence
Daniella Goldfarb, Chemical and Biological Physics Department, Weizmann Institute of Science, Rehovot 76100, Israel.
Email: daniella.goldfarb@weizmann.ac.il

Present address
Annalisa Pierro, Konstanz Research School Chemical Biology, Department of Chemistry, University of Konstanz, Konstanz, Germany.

Funding information
The Helen and Martin Kimmel Institute for Magnetic Resonance Research and the historic generosity of the Harold Perlman Family (D. G.); The Joint NSFC (China)-ISF grant, Grant/Award Number: 3559/21; The "Agence Nationale de la Recherche", Grant/Award Number: ANR-18-CE11-0007-01

Review Editor: Hideo Akutsu

Abstract

The combined effects of the cellular environment on proteins led to the definition of a fifth level of protein structural organization termed quinary structure. To explore the implication of potential quinary structure for globular proteins, we studied the dynamics and conformations of *Escherichia coli* (*E. coli*) peptidyl-prolyl *cis/trans* isomerase B (PpiB) in *E. coli* cells. PpiB plays a major role in maturation and regulation of folded proteins by catalyzing the *cis/trans* isomerization of the proline imidic peptide bond. We applied electron paramagnetic resonance (EPR) techniques, utilizing both Gadolinium (Gd(III)) and nitroxide spin labels. In addition to using standard spin labeling approaches with genetically engineered cysteines, we incorporated an unnatural amino acid to achieve Gd(III)-nitroxide orthogonal labeling. We probed PpiB's residue-specific dynamics by X-band continuous wave EPR at ambient temperatures and its structure by double electron–electron resonance (DEER) on frozen samples. PpiB was delivered to *E. coli* cells by electroporation. We report a significant decrease in the dynamics induced by the cellular environment for two chosen labeling positions. These changes could not be reproduced by adding crowding agents and cell extracts. Concomitantly, we report a broadening of the distance distribution in *E. coli*, determined by Gd(III)–Gd(III) DEER measurements, as compared with solution and human HeLa cells. This suggests an increase in the number of PpiB conformations present in *E. coli* cells,

possibly due to interactions with other cell components, which also contributes to the reduction in mobility and suggests the presence of a quinary structure.

KEYWORDS

DEER, in-cell EPR, PpiB, quinary structure, site-directed spin labeling, unnatural amino acid

1 | INTRODUCTION

In the field of structural biology, it is currently accepted that the intracellular environment, rich with ions, metabolites, and macromolecules, can affect the stability, folding, and function of proteins via macromolecular crowding and different types of interactions with cellular components (Cohen & Pielak, 2017; Ellis, 2001; Freedberg & Selenko, 2014; Guin & Gruebele, 2019; Plitzko et al., 2017; Rivas & Minton, 2018; Zhou et al., 2008). The combined effects of the cellular environment on individual proteins led to the definition of a fifth level of protein structural organization termed quinary structure (Cohen & Pielak, 2017; Guin & Gruebele, 2019; Rivas & Minton, 2018), which appears to have coevolved with protein surface properties to ensure optimal functionality (McConkey, 1982). Extensive theoretical (McGuffee & Elcock, 2010; Rivas & Minton, 2016, 2018; Yu et al., 2016) and experimental efforts have been directed toward understanding and elucidating quinary structure effects for different proteins (see recent reviews (Cheung & Gasic, 2018; Cohen & Pielak, 2017; Guin & Gruebele, 2019; Qin & Zhou, 2017; Rivas & Minton, 2018). To understand the combined effects of the cellular milieu on protein structure, dynamics, stability, and interactions, in-cell measurements are often combined with in vitro measurements under controlled artificial conditions. Nonetheless, the number of in-cell studies is still low owing to the multiple challenges the biophysical techniques experience when applied to cells (Plitzko et al., 2017). Accordingly, cell lysates are often used as surrogate models, yet they often fail to replicate the cellular effects (Dalaloyan et al., 2019; Rivas & Minton, 2018).

To date, most in-cell structural and dynamic studies of proteins employ nuclear magnetic resonance (NMR) (Luchinat & Banci, 2017, 2022; Theillet, 2022), and to a lesser extent, fluorescence spectroscopy (Gruebele & Pielak, 2021; König et al., 2021). Such studies reported on protein folding and stability in cells (Danielsson et al., 2015; Dhar et al., 2011; Ebbinghaus et al., 2010; Gnutt et al., 2019; Guo et al., 2012; Guzman et al., 2014; Monteitha & Pielak, 2014; Schlesinger et al., 2011; Sukenik et al., 2017), structural changes of disordered proteins (Dedmon et al., 2002; Phillip et al., 2012; Theillet et al., 2016), protein association, and the stabilization of oligomeric assemblies (König et al., 2015; Kwapiszewska et al., 2019; Margineanu et al., 2016). More recently, an in-cell NMR study reported that loop conformational dynamics in a globular protein can be modified through weak interactions (Wang, Song, et al., 2023). The addition of other biophysical methods that can provide structural and dynamic information on proteins in cells is essential for gathering the volume of experimental results required for understanding and establishing the quinary structure concept.

Significant progress in developing suitable spin labels and labeling approaches in the last decade has turned electron paramagnetic resonance (EPR) spectroscopy into an attractive method for in-cell exploration of protein structure and dynamics (Bonucci et al., 2020; Galazzo et al., 2022; Giannoulis et al., 2021; Goldfarb, 2022; Hänsel et al., 2014; Igarashi et al., 2010; Jassoy et al., 2017; Martorana et al., 2014; Shenberger et al., 2023; Wang, Fang, et al., 2012). Herein, we applied continuous-wave (CW) EPR and double-electron electron resonance (DEER) methods to explore a potential manifestation of quinary structure on a well-structured globular protein, *Escherichia coli (E. coli)* peptidyl-prolyl *cis/trans* isomerase B (PpiB) in its native milieu, *E. coli* cells (Edwards et al., 1997). PpiB is an important chaperone that plays a key role in the maturation and regulation of folded proteins. PpiB regulates protein folding by catalyzing the *cis/trans* isomerization of the proline imidic peptide bond, which often affects the activity and structure of many folded proteins in the cell (Klein et al., 2020). PpiB has been extensively studied in the past by NMR under in vitro conditions (Abdelkader et al., 2021; Cao et al., 2014; Guignard et al., 2002; Jia et al., 2009; Orton et al., 2021; Ozawa et al., 2004; Ozawa, Dixon, & Otting, 2005; Ozawa, Headlam, et al., 2005; Qianzhu et al., 2020; Su et al., 2011; Takeda et al., 2011; Welegedara et al., 2018; Wu et al., 2007) and recently it has been used as a model protein for developing in-cell DEER approaches (Yang, Pan, et al., 2020). In these studies, the labeled PpiB was delivered into HeLa human cells, which is not its native environment.

The majority of in-cell EPR structural studies of proteins and nucleic acids have been followed by DEER distance measurements using nitroxide (Azarkh et al., 2013; Azarkh, Okle, Eyring, et al., 2011; Azarkh, Okle, Singh,

et al., 2011; Cattani et al., 2017; Collauto et al., 2020; Igarashi et al., 2010; Joseph et al., 2015, 2019; Karthikeyan et al., 2018; Krstić et al., 2011; Singewald et al., 2019), Gadolinium (Gd(III)) (Azarkh et al., 2019; Dalaloyan et al., 2019; Galazzo et al., 2022; Martorana et al., 2014; Qi et al., 2014; Yang et al., 2017, 2018), and trityl (Fleck et al., 2020; Jassoy et al., 2017; Yang, Pan, et al., 2020) spin label pairs. Owing to the sensitivity of nitroxide spin labels to cellular reduction (Azarkh, Okle, Eyring, et al., 2011; Krstić et al., 2011; Wang, Zhang, et al., 2023), efforts have been made to design and synthesize nitroxide spin labels that are reduction resistant (Bleicken et al., 2019; Collauto et al., 2020; Jagtap et al., 2015; Karthikeyan et al., 2018) concurrently to the development of delivery methods that rely on a minimal time for cell recovery for *E. coli* (Pierro et al., 2022; Torricella et al., 2021). Moreover, endeavors to achieve in-cell cytosolic labeling are under development (Jana et al., 2023; Kugele et al., 2021; Schmidt et al., 2014; Widder et al., 2020). Although Gd(III) and trityl spin labels are preferred over nitroxide spin labels, owing to their higher in-cell stability, they lack the ability to provide information about the spin label dynamics, which is readily obtained with nitroxides. In principle, orthogonal nitroxide-Gd(III) labeling of a protein can provide in a single sample both structural and dynamic information (Garbuio et al., 2013).

In this work, we employed several labeling approaches to explore the residue-specific reorientational dynamics as well as structural characteristics of PbiB in *E. coli* cells as compared with solution. This includes nitroxide-Gd(III) orthogonally labeled PpiB generated via the introduction of an unnatural amino acid (UAA) residue conjugated to a Gd(III) label (Abdelkader et al., 2015; Garbuio et al., 2013) and a genetically encoded cysteine residue attached to a shielded nitroxide label termed M-TETPO (Karthikeyan et al., 2018) (Figure 1). M-TETPO has been shown to be less prone to cellular reduction compared with the standard nitroxide spin labels (Karthikeyan et al., 2018; Wang, Zhang, et al., 2023). In addition, singly and doubly nitroxide-labeled PpiB variants, as well as a doubly labeled Gd(III) one, were used for control and comparison purposes. The selected labeling sites in each variant were situated on a loop and a helix, both solvent-exposed, to explore different structural elements. We found that PbiB undergoes a considerable reduction in the residue-specific mobility in the cell for both labeling positions, as compared with solution conditions. Furthermore, the *E. coli* in-cell Gd(III)–Gd(III) distance distribution was broader than in

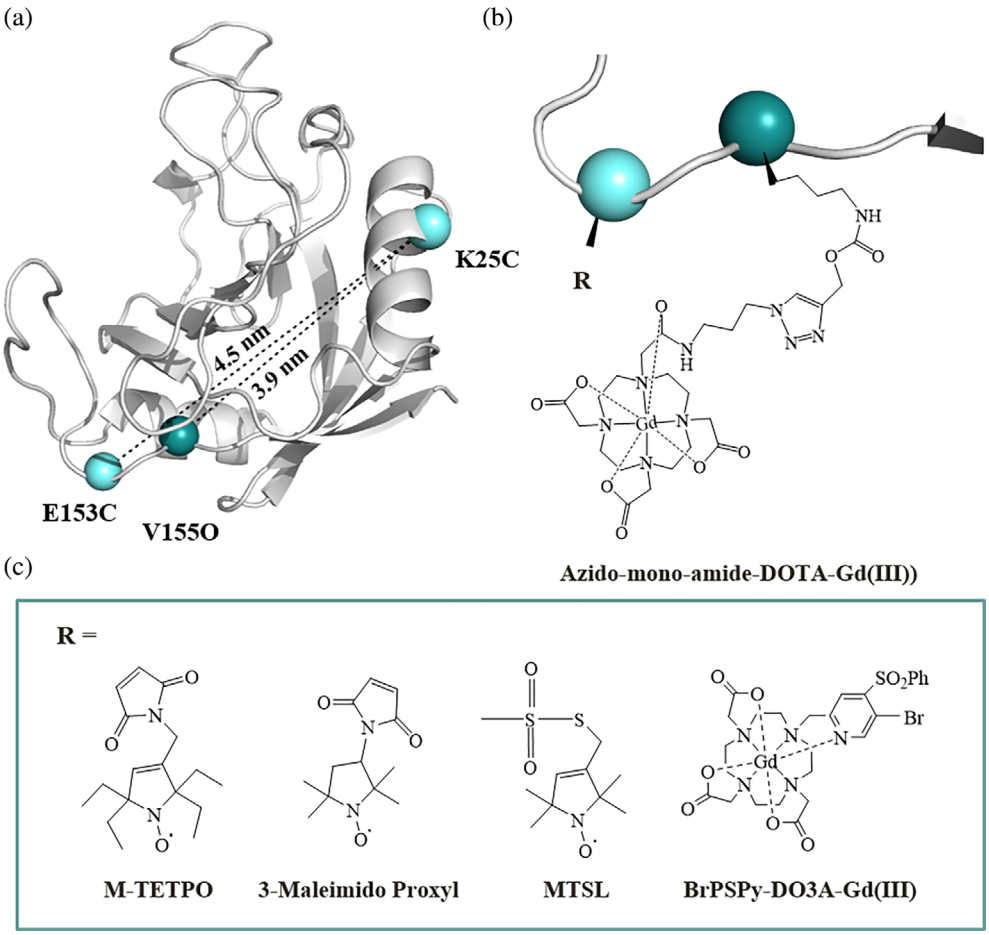

FIGURE 1 Peptidyl-prolyl *cis/trans* isomerase B (PpiB) crystal structure and spin labels used in this study. (a) Crystal structure of PpiB (PDB:2NUL) (Edwards et al., 1997), showing the chosen labeling sites of PpiB(K25C/E153C) and PpiB(K25C/V155O, where O stands for pyrro-L-lysine [Pyl]) variants, along with the expected distances from the corresponding Cα carbons, obtained from PyMOL software. (b) Genetically engineered cysteine (cyan), with conjugated spin label R, and the incorporated Pyl (dark green) with its sidechain coupled to the Gadolinium (Gd(III)) label. (c) The spin label agents used in this work for conjugation via a cysteine residue.

solution and in HeLa cells samples. This indicates the presence of a larger number of PpiB's conformations in *E. coli* probably due to specific or nonspecific interactions with cellular partners, which subsequently, contribute to the restriction of the protein dynamics and suggest the existence of PpiB's quinary structure.

2 | RESULTS

2.1 | The labeled samples

Following earlier work (Yang, Pan, et al., 2020), we decided to investigate the double-cysteine PpiB variant K25C/E153C, where K25C is located on a helix and E153C on a loop motifs (Figure 1). These sites were labeled with pairs of BrPSPy-DO3A-Gd(III) (DO3A-Gd (III)) (Yang et al., 2018), M-TETPO (Karthikeyan et al., 2018), and 3-maleimido-proxyl (3-MSL) spin labels (Figure 1) and these are referred to as PpiB(K25C/E153C)-DO3A-Gd(III), PpiB(K25C/E153C)-M-TETPO and PpiB(K25C/E153C)-3-MSL, respectively. To implement the orthogonal Gd(III)-nitroxide labeling approach and to facilitate the comparison with the above mentioned samples, we generated an additional PpiB variant, replacing V155 on the loop with the alkene-containing lysine-based pyrrolysine (Pyl, O) UAA, referred to as PpiB(K25C/V155O). The UAA residue was then tethered to a Gd(III) spin label (Figure 1b) via "click" chemistry utilizing the Cu(I)-catalyzed alkene/azide cycloaddition reaction (Figure 1) (Milles et al., 2012). The produced variants were characterized by differential scanning fluorimetry (nano-DSF) and mass spectrometry Time-of-Flight Electrospray Ionization mass spectrometry (TOF-IES) (Figures S1 and S2). Subsequently, two nitroxide-Gd(III) samples were prepared: One labeled with M-TETPO, which is suitable for in-cell measurements (Karthikeyan et al., 2018), referred to as PpiB(K25C/V155O)-Azido-Gd(III)/M-TETPO, and the other with *S*-(1-oxyl-2,2,5,5-tetramethyl-2,5-dihydro-1H-pyrrol-3-yl)methyl methanesulfonothioate (MTSL), termed PpiB(K25C/V155O)-Azido-Gd(III)/MTSL, which was used as a reference. In addition, we prepared a sample of PpiB(K25C/V155O)-M-TETPO, labeled only with M-TETPO to explore specifically the nitroxide dynamics of the cysteine positioned on a helix at position 25.

2.2 | CW EPR and DEER on solution samples

We began characterizing the PpiB variants in solution and measured room temperature X-band CW EPR to examine the local dynamics at the two nitroxide labeling sites. The spectrum of PpiB(K25C/E153C)-M-TETPO (Figure 2) is typical of a fast rotational diffusion for both labeling sites. This was further confirmed by the spectrum of PpiB(K25C/V155O)-M-TETPO, having a spin label only at position 25 (Figure 2). Surprisingly, PpiB(K25C/V155O)-Azido-Gd(III)/M-TETPO exhibited an EPR spectrum which is a superposition of M-TETPO undergoing fast and slow motion, with a dominant population of the latter (Figure S3). The same behavior was observed for PpiB(K25C/V155O)-Azido-Gd(III)/MTSL. We do not know the reason for the change in the nitroxide mobility; however, we speculate that it originated from the presence of a Cu(II)-His_6 tag complex in the nitroxide's vicinity, formed during the click chemistry reaction (more details in the Supplementary Information).

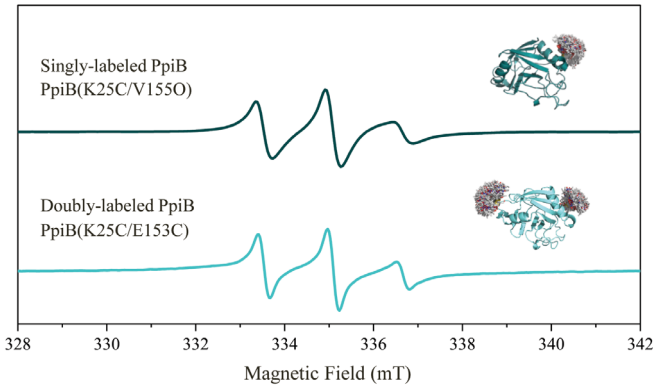

FIGURE 2 Room temperature X-band continuous-wave electron paramagnetic resonance (EPR) spectra of M-TETPO doubly labeled peptidyl-prolyl *cis/trans* isomerase B (PpiB) (K25C/E153C) (cyan) versus M-TETPO singly labeled PpiB(K25C/V155O) (dark green) along with the corresponding crystal structure of PpiB (PDB:2NUL) (Edwards et al., 1997) with the M-TETPO rotamers at the selected labeling sites obtained with MtsslSuite online available software (Hagelueken et al., 2013).

Next, we performed W-band Gd(III)-nitroxide DEER distance measurements on orthogonally labeled PpiB (K25C/V155O). The distance distribution serves as a signature of the protein conformation and can be compared with earlier reports (Yang, Pan, et al., 2020). The DEER traces and the corresponding distance distributions of PpiB(K25C/V155O)-Azido-Gd(III)/M-TETPO reveal a relatively narrow distance distribution despite the relatively long Gd(III) tether (Figure 1). The maximum distance distribution, at 4.5 nm, is in good agreement with earlier Gd(III)-Gd(III) DEER reports (Yang, Pan, et al., 2020). The modulation depth of 12% confirms the high labeling efficiency of M-TETPO based on earlier measurements acquired on our spectrometer (Jash et al., 2022). The PpiB(K25C/V155O)-Azido-Gd(III)/MTSL showed a slightly

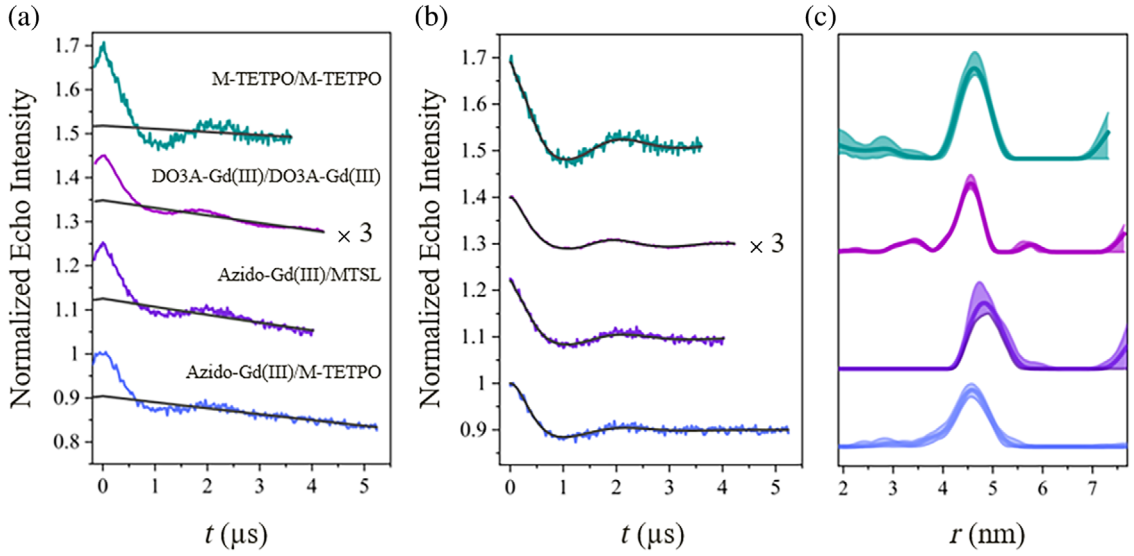

FIGURE 3 Solution W-band double electron–electron resonance (DEER) traces of peptidyl-prolyl *cis/trans* isomerase B (PpiB) variants labeled with different spin labels pairs, as depicted in (a). (a) Primary DEER data with the background correction function. (b) The DEER traces after background correction with the fit. (c) The corresponding distance distributions. The shaded areas above and below the main distance distribution line represent ±2 standard deviations of the distributions calculated using the validation option in the DeerAnalysis software (Jeschke et al., 2006). The *y* axes of PpiB(K25C/E153C)-DO3A-Gadolinium (Gd(III)) in (a) and (b) were threefold multiplied for comparison purposes and all traces were shifted upstream for clarity. MTSL, *S*-(1-oxyl-2,2,5,5-tetramethyl-2,5-dihydro-1H-pyrrol-3-yl)methyl methanesulfonothioate.

shifted distance distribution, with a maximum at 4.7 nm, which we attribute to the different linkers of the two nitroxide labels, and a modulation depth (9.6%) slightly lower than with M-TETPO. As control experiments, PpiB(K25C/E153C)-M-TETPO and PpiB(K25C/E153C)-DO3A-Gd(III) were measured as well (Figure 3). As expected, both spin-labeled variants exhibit a similar distance distribution centered at 4.5 nm. These results show that although the nitroxide's motional freedom was affected by the Gd(III) labeling, the obtained distance distributions remained as expected and proved that the PpiB structural elements probes by these labeling sites were not disturbed. This supports our suggestion of the His_6 tag involvement in the restriction of the nitroxides' motion.

2.3 | In-cell EPR and DEER

So far, most in-cell EPR studies have been carried out on proteins delivered by electroporation (EP) into mammalian cells (Dalaloyan et al., 2019; Jassoy et al., 2017; Martorana et al., 2014; Theillet et al., 2016; Yang et al., 2017, 2018, 2019; Yang, Chen, et al., 2020; Yang, Pan, et al., 2020) or injected into *Xenopus laevis* oocytes (Azarkh et al., 2019; Azarkh, Okle, Singh, et al., 2011; Cattani et al., 2017; Igarashi et al., 2010). As PpiB is an *E. coli* protein, we aspired to conduct the EPR measurements in its physiological milieu. Recently, it has been shown that maleimido proxyl doubly labeled NarJ was delivered into *E. coli* cells by EP and subsequent X-band CW EPR measurements of various variants were successfully carried out (Pierro et al., 2022). Following this work, we further optimized the EP protocol for spin-labeled PpiB incorporation into *E. coli* cells, using confocal fluorescence microscopy of fluorescent-labeled Atto-488 PpiB(K25C/E153C), as described previously (Martorana et al., 2014) (Figure 4 and Figures S4 and S5). Notably, the combination of freshly prepared competent cells and the addition of 2 mM ATP dramatically increased the protein delivery yields. Using this protocol, the time between the application of the EP pulse and the beginning of the recording of the CW-EPR spectrum or freezing the sample for DEER measurements was 20 min. Cell viability assay indicated approximately a 30% loss of living cells (Figure S6), similar to earlier reports (Pierro et al., 2022; Torricella et al., 2021).

To eliminate the possibility of the external association of the labeled protein with the outer cell membrane, we prepared a control sample where the protein was delivered without the EP pulse. The control sample showed only weak fluorescence intensity arising mostly from the autofluorescence of the cells themselves (Figure S5) and had no EPR signal. These results confirmed the presence of the labeled protein inside the cells, while all the external PpiB was removed by the extensive washings.

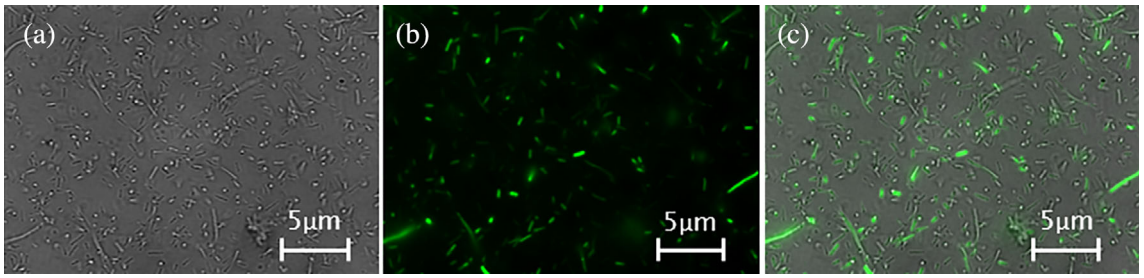

FIGURE 4 Confocal microscopy images showing the delivery of fluorescently labeled ATTO-488 doubly labeled peptidyl-prolyl *cis/trans* isomerase B (PpiB) (K25C/E153C) into *Escherichia coli* cells. (a) Bright field, (b) confocal fluorescence microscopy (473 nm), and (c) the alignment of both images.

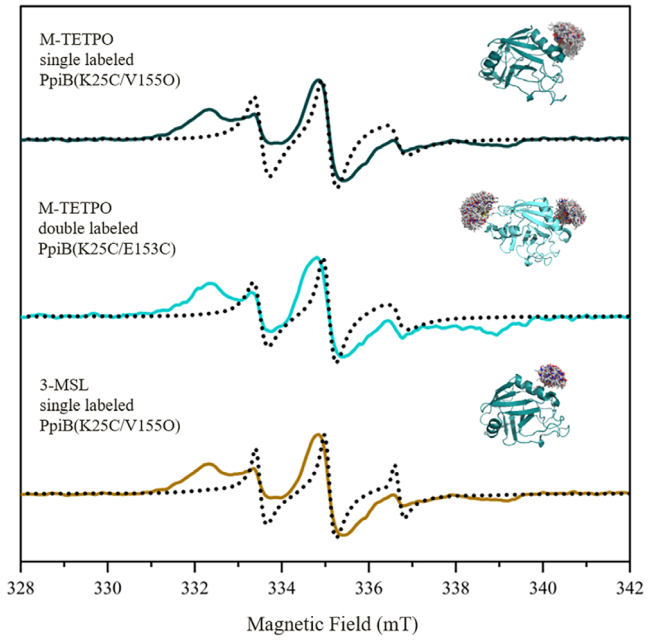

FIGURE 5 X-band continuous-wave electron paramagnetic resonance (EPR) spectra of 3-maleimido-proxyl (3-MSL) (brown) and M-TETPO (green) singly labeled peptidyl-prolyl *cis/trans* isomerase B (PpiB) (K25C/V155O) and M-TETPO doubly labeled PpiB(K25C/E153C) (cyan) in *Escherichia coli* cells compared with the spectra in solution (gray lines). The crystal structure of PpiB (PDB:2NUL) (Edwards et al., 1997) with the rotamers of the spin labels are shown on the right.

The X-band CW EPR of PpiB(K25C/E153C)-M-TETPO in *E. coli* cells had a line shape significantly different from the solution spectra. It changed from a line shape characteristic of high mobility to a practically rigid limit spectrum (Figure 5) showing that in the cell, the motions of both nitroxides, at positions 25 (helix) and 153 (loop), were restricted. This was further confirmed by the spectrum of singly labeled PpiB(K25C/V155O)-M-TETPO delivered into the cells, revealing again a transition of the highly mobile spin label at position 25 to an immobile state (Figure 5).

To track the in-cell stability of the nitroxide labels, we recorded the CW EPR spectra of PpiB (K25C/V155O)-M-TETPO and PpiB(K25C/V155O)-3-MSL as a function of time (Figure 6). We observed an 80% peak-to-peak signal loss of the central hyperfine peak for 3-MSL over 60 min, whereas for M-TETPO, it decreased by only 10% within a similar time. The reduction of 3-MSL serves as an additional evidence for the presence of PpiB inside the cells.

In an attempt to resolve the origin of the observed increase in the rotational correlation time, we examined the effect of crowding agents on the spectrum of PpiB(K25C/V153C)-M-TETPO using Ficoll (300 mg/mL), lysozyme (30 mg/mL), and bovine serum albumin (200 mg/mL) featuring neutral charge and proteins with negative and positive charges, respectively (Rivas & Minton, 2016; Wang, Sarkar, et al., 2012). The CW-EPR spectra reveal only a minor population of spin labels experiencing slow motion for all three samples (Figure S7), with the addition of Ficoll showing the least change. We note, however, that the crowding in the cell may be significantly higher than the mimetic conditions tested.

To explore the effect of potential binding partners on the nitroxide dynamics, we added PpiB(K25C/V153C)-M-TETPO (100 μM) to *E. coli* cell extract (25 mg/mL protein concentration) and recorded the spectra as a function of time (Figure S8). Previous studies on PpiB revealed multiple binding partners in the cell, as expected for a dominant cytosolic chaperone (Klein et al., 2020; Skagia et al., 2016) and, therefore, we expected to observe changes. The spectra did not reveal the same changes observed in the cell, yet they did exhibit a significant contribution of a slow-motion component. In addition, we observed a rapid decrease in the EPR signal as a function of time due to the nitroxide reduction, at a rate much faster than in the cell, as reported earlier for another protein (Bleicken et al., 2019; Jagtap et al., 2015; Karthikeyan et al., 2018; Wang, Zhang, et al., 2023). By normalizing the spectra to allow for line-shape comparison, we detected minimal changes in the line shape with time

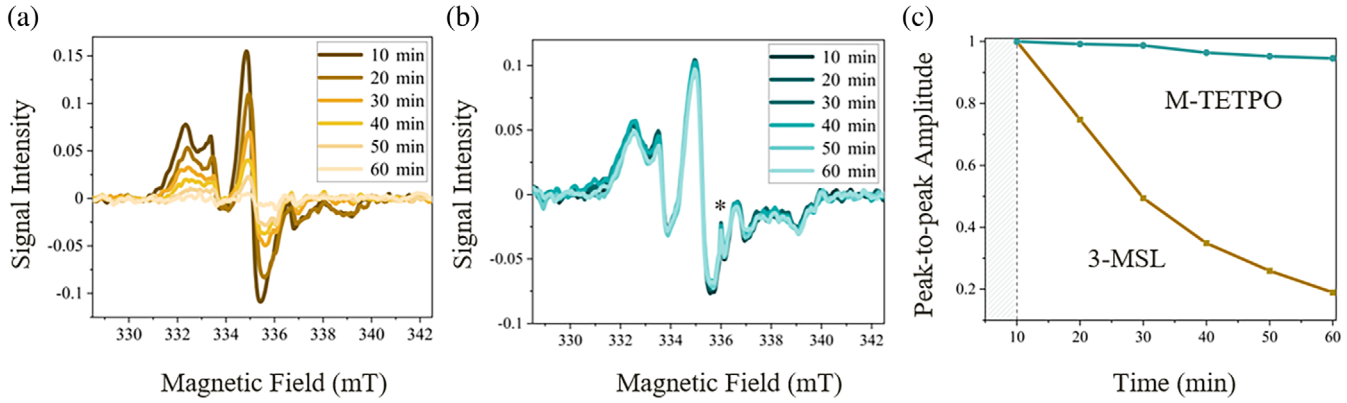

FIGURE 6 X-band continuous-wave electron paramagnetic resonance (EPR) spectra of (a) 3-maleimido-proxyl (3-MSL) and (b) M-TETPO singly labeled peptidyl-prolyl *cis/trans* isomerase B (PpiB) (K25C/V155O) in *Escherichia coli* cells as a function of time. Zero time corresponds to the insertion time of the sample into the spectrometer, which was approximately 20 min after electroporation (EP). (c) The peak-to-peak amplitude of the central peak as a function of time (derived from [a, b]). The spectrum's acquisition time was 10 min (grey region in the Figure) due to the low signal-to-noise ratio, characteristic of the in-cell samples, and therefore, the first spectrum is set to 10 min. The asterisk denotes cavity background signals.

and the decay rates of the fast and slow motion components were similar (Figure S8).

Next, we performed in-cell DEER measurements to determine whether the change in the dynamics is associated with a structural change. Our attempts to deliver PpiB(K25C/V155O)-Azido-Gd(III)/M-TETPO into *E. coli* cells, which would allow in-cell probing of both dynamics and structure on one sample, did not succeed. The delivery efficiency of PpiB into *E. coli* by EP is rather low, ~4.2%–7.2%, as estimated from the echo intensity of PpiB(K25C/E153C)-DO3A-Gd(III), the CW-EPR results, and earlier reports (Pierro et al., 2022; Torricella et al., 2021). Therefore, for a sufficient amount of in-cell protein to be DEER detectable, the PpiB concentration in the EP buffer should be 0.35 mM or higher, taking into account that the additions to the EP mixture result in a two-fold dilution. Unfortunately, PpiB(K25C/V155O)-Azido-Gd(III)/M-TETPO precipitated at these high concentrations. Interestingly, this precipitation was observed only upon Gd(III)-labeling of PpiB(K25C/V155O). As we mentioned earlier, we suspect that it is due to the interaction of the His_6-tag with the Cu(II), as described in the Supplementary Information. Therefore, to detect changes in the conformation of PpiB induced by the cellular environment, we delivered PpiB(K25C/E153C)-DO3A-Gd(III) into *E. coli* cells and carried out Gd(III)-Gd(III) DEER measurements.

The echo-detected EPR spectrum of PpiB(K25C/E153C)-DO3A-Gd(III) in *E. coli* cells shows a clear Gd(III) signal superimposed on that of endogenous Mn(II) naturally present in the cell (Martorana et al., 2014) (Figure S9B). The corresponding echo decays, compared with the solution samples, are shown in Figure S10. A high-quality in-cell DEER trace (Figure 7) was obtained only when the external protein concentration in the EP mixture was 350 μM protein (repeats are shown in Figure S11). For comparison, delivery into mammalian cells (human cervical cancer [HeLa] cells) by EP required 250 μM (Martorana et al., 2014; Theillet et al., 2016; Yang et al., 2018). The maximum of the distance distribution in *E. coli* matched that in solution samples (at 4.5 nm), yet it exhibited a broader distribution (Figure 7). Interestingly, the same labeled protein in HeLa cells gave a width similar to the solution samples, in agreement with earlier reports (Yang, Pan, et al., 2020). Hence, the broadening of the distance distribution might suggest a different structural behavior specific to *E. coli* cells. We also delivered M-TETPO labeled PpiB into HeLa cells, but after the required 4 h cell recovery time, there was no EPR signal. Accordingly, we could not compare the dynamic behavior of spin-labeled PpiB in *E. coli* and in HeLa cells due to the longer recovery time required for HeLa cells (Theillet et al., 2016).

3 | DISCUSSION

The comparison of the CW-EPR and DEER results in solution and in *E. coli* cells revealed a considerable reduction of the nitroxide spin label dynamics at both surface-exposed positions, 25 and 153, located on helix and loop motifs, respectively. Moreover, we observe a broadening of the Gd(III)–Gd(III) distance distribution upon delivery into *E. coli* cells, which was not observed in HeLa cells.

The detection of a significant restriction in the nitroxide mobility in *E. coli* cells of both 3-MSL and M-TETPO at the 25 and 153 positions could, in principle, be attributed to a simple picture where the tumbling of the

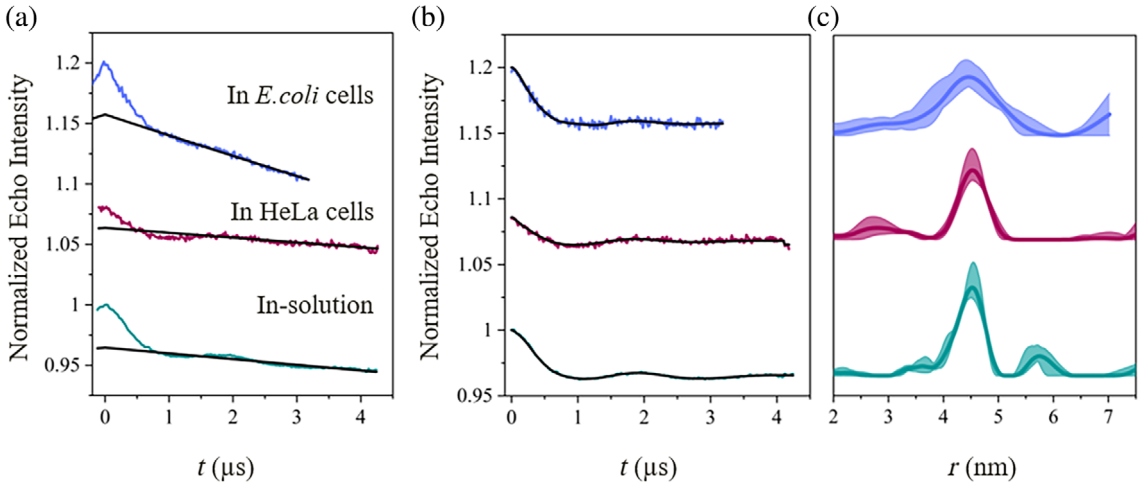

FIGURE 7 Double electron–electron resonance (DEER) traces of peptidyl-prolyl *cis/trans* isomerase B (PpiB) (K25C/E153C)-DO3A-Gadolinium (Gd(III)) in solution (green), in HeLa (red), and in *Escherichia coli* (blue) cells. (a) Primary DEER experimental data with the background function (black). (b) DEER traces after background removal with the fit in black. (c) The corresponding distance distributions. The shaded areas above and below the main distance distribution line represent the ±2 standard deviations of the distributions calculated using the validation option in the DeerAnalysis software (Jeschke et al., 2006). All traces were shifted upwards to facilitate the comparison.

protein in solution is fast, leading to a fast motion spectrum, whereas the viscosity in the *E. coli* is much higher, slowing the tumbling rate considerably. However, we ruled out this explanation since it could not be reproduced with artificial crowding agents and recent reports of fast-motion EPR spectra of proteins with molecular weights higher than those of PpiB in *E. coli* (Torricella et al., 2021). Furthermore, a recent CW-EPR study on the NarJ chaperone in *E. coli* reported changes in the spin label local mobility, depending on the location of the spin label in the protein. For some NarJ variants, a significant restriction of the nitroxide's motion was observed, whereas for others, the difference was subtle (Pierro et al., 2022). The effect of the cell environment on local dynamics in proteins has also been recently reported for the loop dynamics of GB3 in *E. coli* cells (Wang, Song, et al., 2023). The observed restriction could not be reproduced by the addition of cell extract either, which suggests that it is not only caused by specific interactions with partners in the spin labels vicinity. The difficulty in reproducing the protein dynamics behavior in solution emphasizes the importance of in-cell studies.

Interestingly, the background decay of the DEER trace of the *E. coli* sample was stronger than that of the HeLa cell sample, although the total in-cell concentration in *E. coli* was lower, as determined from the echo intensity. This indicates a higher local concentration of the labeled protein that could result from the limited available cell volume of small bacterial cells and their higher protein content. Differences were also observed in the DEER distance distribution, which has the same distance distribution maxima, yet with a larger width, compared with the HeLa cells and solution DEER data. While comparing to the HeLa cell results, we should consider that specific or nonspecific interactions of PpiB with native cell components forming the quinary structure may not be present in HeLa cells since PpiB is not a human protein. Hence, this broadening may suggest a larger ensemble of conformations of the Gd(III) label and/or the residue it anchored to (Heubach et al., 2023), owing to the quinary structure. The broader range of conformations together with the high local viscosity are, therefore, manifested in the slower exchange rate between the various conformers which is insufficient for averaging the nitroxide anisotropic magnetic interactions. In principle, a rigid limit CW-EPR spectrum could also arise from a single, well-defined conformation of the spin label. This, however, would lead to a narrower distance distribution as opposed to the broader one that we observed. Moreover, we verified that the broadening of the distance distribution does not originate from the stronger background decay, which can lead to a faster decay of the dipolar modulations. Thus, we multiplied the solution data with the *E. coli* background decay and did not observe a broadening in the derived distance distribution.

Our original idea to use one sample with orthogonal Gd(III)-nitroxide labeling to probe both the dynamics and structure in the cell did not succeed and we had to proceed with two samples. We noted that the reduced M-TETPO in the cell was not a major issue, given the fast delivery and cell recovery approach used. The main difficulty was in obtaining a sufficiently high concentration of the orthogonal Gd(III)-nitroxide-labeled PpiB(K25C/V155O) in the EP buffer, required to achieve the needed in-cell concentration for DEER. If indeed the problem originates from the presence of the His_6 tag, it can be overcome by simply removing it. This, however, does not

abolish the need for high concentrations that can be an issue for many proteins. Nevertheless, PpiB(K25C/V155O) variant was very useful for following the behavior of a singly labeled M-TETPO PpiB in the cell by CW-EPR.

4 | CONCLUSIONS

Here, we explored the structure and dynamics of PpiB in its native environment, *E. coli* living cells, combining CW-EPR and W-band DEER. We observed by X-band CWEPR a significant decrease in the nitroxide spin label rotational diffusion rate at two labeling positions, 25 situated on a helix and 153 on a loop, in the cell, compared with in solution. Attempts to mimic this effect with several crowding agents and *E. coli* cell lysate failed to reproduce the significant change in local mobility, emphasizing the importance of in-cell measurements. In-cell DEER measurements carried out on PpiB labeled with Gd(III) spin labels at positions 153 and 25 revealed the same maxima of the distance distribution as in solution and HeLa cells, yet exhibited a broader distribution. The broadening of the distance distribution suggests an increase in the number of conformations owing to interactions (specific and/or nonspecific) with cell components, suggesting the presence of quinary structure as well as local crowding. These interactions are also responsible for the decrease in the exchange rate between various conformations of the nitroxide labels.

5 | MATERIALS AND METHODS

5.1 | Protein expression and purification

5.1.1 | PpiB(K25C/E153C)

The double-cysteine PpiB mutant was produced, as described earlier (Yang, Pan, et al., 2020).

5.1.2 | PpiB(K25C/V155O)

To expand the genetic code and produce the UAA-incorporated PpiB mutants, we followed the available literature procedures (Liu & Schultz, 2010; Wang, Fang, et al., 2012). Briefly, the "amber" nonsense codon was reassigned for UAA incorporation and cloned at chosen positions to produce the following mutants: PpiB(K25C/E153O), PpiB(K25C/D154O), PpiB(K25C/V155O, and PpiB(K25C/A140O). Generating four different mutants was necessary since incorporation yields strongly depend on the incorporation position in the protein. Cloning was performed using the Q5 site-directed mutagenesis Kit (New England Biolabs), and mutations were verified using DNA sequencing.

The cloned plasmids were cotransformed into *E. coli* BL21 (DE3) competent cells with the system plasmid pEVOL-Pyl bearing chloramphenicol resistance (Tyagi & Lemke, 2013). The system plasmid contains the genes expressing the orthogonal pair of aminoacyl-transfer RNA (tRNA) synthetase (pyIRS)/amber suppressor tRNA required for specific and selective incorporation of pyrro-L-lysine (Pyl, O) (Iris Biotech GMBH). Pyl was nicely incorporated into all selected mutants; however, the PpiB (K25C/V155O) mutant showed high expression levels and was selected for further use. *E. coli* BL21 (DE3) cells, harboring the system plasmid (pEVOL-Pyl) and the selected PpiB mutant (pET_3a-His_6-PpiB(K25C/V155O), were grown at 37°C and 220 rpm in Luria broth (LB) broth medium supplemented with 100 mg/mL ampicillin, 34 mg/mL chloramphenicol, and 0.2% (w/v) arabinose to preinduce the aminoacyl-tRNA synthetase/amber suppressor tRNA pair. After $OD_{600} = 0.8$ was reached, the cell culture was cooled, supplemented with 2 mM Pyl (Iris Biotech GMBH), and transferred to 20°C, 220 rpm for 15 min. Protein induction was generated by 1 mM IPTG overnight (~16 h). The cells were harvested by centrifugation (6000×*g* at 4°C for 10 min), following lysis using a French press homogenizer (25,000 psi, 3 cycles) after resuspension with 50 mM Tris–HCl (pH = 7.5) containing 300 mM NaCl, 2 mM $MgCl_2$, and 10 μg/mL Benzonase (Novagen). Once the cell debris was removed by centrifugation (16,000×*g* at 4°C for 1 h), the supernatant was subjected to fractionation via a Ni-NTA HisTrap FF column (GE Healthcare), followed by a size-exclusion column using a HiLoad 16/600 Superdex 75 column (GE Healthcare). Verified fractions containing pure protein were collected and concentrated. The pure protein was aliquoted, snap-frozen in liquid nitrogen, and stored at −80°C.

5.2 | Protein labeling

5.2.1 | BrPSPy-DO3A-Gd(III) (DO3A-Gd(III)) labeling

DO3A-Gd(III) synthesis and labeling was performed as reported earlier (Yang et al., 2018).

5.2.2 | MTSL, 3-MSL, and M-TETPO labeling

Commercial spin label, MTSL (Chem Cruz Biothecnologies, Inc.) and 3-MSL (Sigma) were used. The M-TETPO spin label was synthesized and conjugated to cysteine residue as described (Karthikeyan et al., 2018).

The protein was treated with 1 equivalent of tris(2-carboxyethyl)phosphine (TCEP) at 4°C for 30 min. Once the reducing agent was removed using a desalting column, 10-fold (per cysteine residue) of the commercial nitroxide spin label was added gradually to the protein in 50 mM Tris–HCl (pH = 7.5), and the mixture was incubated at 4°C overnight (~16 h) in the dark. For Gd(III)-nitroxide labeling of the PpiB(K25C/V155O) mutant, 1 mM dithiothreitol, or 1 equivalent of TCEP was added during the buffer exchange process after generating the click reaction and prior to the second nitroxide labeling.

5.2.3 | Azido-mono-amide-DOTA-Gd(III) (Azido-Gd(III)) labeling

PpiB(K25C/V155O) was first labeled with Gd(III) to avoid complications arising from nitroxide reduction under the click chemistry conditions.

Conjugating the Azido-Gd(III) spin label to the Pyl (O) via click chemistry was performed following a published protocol (Abdelkader et al., 2015; Loh et al., 2013). To 0.05 mM protein in 50 mM sodium phosphate buffer (pH = 7.5), 150 mM NaCl, 5 mM aminoguanidine, 0.5 mM glycerol, 0.3 mM $CuSO_4$, 1.5 mM 2-[4-({bis[(1-tert-butyl1H-1,2,3-triazol-4-yl)methyl]amino} methyl)-1H-1,2,3-triazol-1-yl]acetic acid (Iris Biotech GMBH) (Besanceney-Webler et al., 2011), and 5 mM ascorbic acid were added. A fivefold per labeling site of the Gd(III) chelate was added to the mixture, following incubation of 3 h at room temperature under rotation. The reaction was performed in a home-built N_2 flow chamber to remove oxygen at the reaction vicinity to reach a higher labeling efficiency. The reaction was terminated by the addition of 2 mM ethylenediaminetetraacetic acid tetrasodium salt dihydrate and rotating for 1 h at room temperature. The click reaction reagents were removed by washing 4 times with 50 mM sodium phosphate buffer (pH = 7.5). SDS-PAGE analysis, based on Tricine (Schägger, 2006), was performed to gain the high-resolution and accurate protein analysis needed for labeling yield determination (Figure S1C). The extent of the labeling efficiency was readily detected by an upstream shift of the purified protein band analyzed on a Tricine-based SDS-PAGE. Finally, we obtained ~90% labeling efficiency, confirmed by mass spectrometry (Figure S2).

5.2.4 | Atto-488 labeling

The fluorophore (Atto-488, Sigma) was added to the protein mixture at a final concentration of 5 mM after reducing the protein by adding 1 equivalent of TCEP, incubating for 30 min at 4°C, and removing the reducing agent by a desalting column (Bio-Rad Laboratories, Ltd.). The labeling reaction was incubated for 2 h at 4°C while rotating.

The labeling process for all variants was always finalized with buffer exchange twice using a Micro Bio-Spin 6 Size Exclusion Spin Column (Bio-Rad Laboratories, Ltd.) to remove the free spin label. The second buffer exchange was with 20 mM Tris–HCl (pH = 7.5), D_2O-based, for pulse-EPR measurements, unless stated otherwise.

5.3 | Protein delivery to living cells

5.3.1 | Incorporation into *E. coli* cells

EP delivery of the labeled protein into *E. coli* DH5α cells New England Biolabs (NEB), was performed as described earlier (Pierro et al., 2022) with minor modifications. Fresh *E. coli* DH5α competent cells were generated before every protein delivery experiment. Overnight cell culture was diluted to $OD_{600} = 0.01$ and grown at 37°C, 220 rpm, until reaching $OD_{600} = 0.9$. Bacterial growth was terminated by incubating the cell culture in an ice bath for 1 h. Then, the cells were harvested by centrifugation (4000×*g*, at 4°C, for 10 min) and washed four times in precooled 10% glycerol buffer with reducing volumes. The cell pellet was resuspended using the same buffer, to reach a cell concentration of $\sim 2\times10^{11}$ cells/mL determined using colony forming units (CFU) LB–agar analysis.

Prior to the addition of 0.25 or 0.35 mM labeled protein and 2 mM ATP to freshly prepared *E. coli* DH5α competent cells, the labeled protein was buffer exchanged to low-salt buffer (10 mM Tris–HCl, pH = 7.5). Then, the mixture was transferred to a 2 mm cuvette (Sigma) and subjected to an electrical pulse (1.8 kV V/cm, 200 Ω, 25 μF, 1 msec pulse) using a BioRad EP generator. Immediately, a prewarmed SOC medium was added to promote fast recovery of the cells following a short incubation at 37°C with 220 rpm for 3 min. Subsequently, the cells were subjected to four wash cycles in PBS buffer, while the first contained 0.005% Triton.

5.3.2 | Incorporation into HeLa cells

Mammalian cervical cancer cells derived from humans (HeLa) were cultured and the labeled protein was delivered by EP following the reported protocol (Martorana et al., 2014; Theillet et al., 2016).

5.4 | CFU determination

After generating fresh *E. coli* DH5α competent cells as described earlier (see Section 5.3.1.), cells were diluted 8 times by a factor of 10-fold in prewarmed LB medium. The 10^6 and 10^8 dilutions were plated on an LB-agar plate and incubated at 37°C for overnight growth. Finally, the number of colonies was numerically evaluated, and the initial CFU number was calculated.

5.5 | Cell viability assay

Fresh *E. coli* DH5α competent cells were treated as described earlier (Pierro et al., 2022) (see Section 5.3.1.). Cells were also mixed with an unlabeled protein in low-salt buffer (10 mM Tris–HCl, pH = 7.4) or without the protein as a control. Then, the cells were diluted by 10-fold six times in LB medium and a drop assay was generated by placing a 3 μL drop of each dilution on a LB-agar plate. Every sample was triplicate-seeded to prevent incoherence measurements. At the highest dilution exhibiting separated colonies, the number of colonies was determined and the initial cell number was evaluated.

5.6 | Sample preparation for EPR measurements

For solution CW EPR, the protein was diluted with a suitable buffer to obtain a protein concentration equal to 100 μM and transferred to a 0.8 mm ID × 1.00 OD EPR quartz capillary. For in-cell measurements, after the last wash cycle, the cells were resuspended with PBS buffer, transferred to a 0.8 mm ID × 1.00 OD EPR quartz capillary and centrifuged (6000×*g* at 4°C for 5 min) to pellet down the cells.

For DEER measurements on solution samples, the labeled protein stock was diluted using D_2O-based 20 mM Tris–HCl (pH = 7.5) to reach a 75–100 μM protein final concentration. At a low protein stock concentration, the spin-labeled protein was buffer exchanged to the same buffer using a desalting column. The final mixture was supplemented with glycerol-d_8 (7:3, v/v), transferred to an EPR quartz capillary (0.6 ID × 0.84 OD mm), flash-frozen in liquid nitrogen, and kept at −80°C.

For DEER measurements on bacterial cell samples, cells were washed two more times with D_2O-based PBS buffer containing glycerol-d_8 (7:3, v/v). Then, the cells were resuspended and transferred to an EPR quartz capillary (0.6 ID × 0.84 OD mm). Finally, the cells were pelleted down by centrifugation (6000×*g* at 4°C for 15 min), flash-frozen in liquid nitrogen, and kept at −80°C.

For DEER measurements on human cell samples, we follow a reported protocol (Yang, Pan, et al., 2020).

5.7 | Estimation of the in-cell spin concentration

By comparing the Gd(III) echo intensity of the in-cell *E. coli* sample to a series of calibrated Gd(III) standard solutions ($GdCl_3$), we estimated that the bulk spin concentration is 15–20 μM. The in-cell concentration is probably higher, considering that the cells do not occupy the full volume of the EPR active volume of the capillary.

5.8 | EPR spectroscopic measurements

CW-EPR measurements were carried out on an X-band Bruker E500 spectrometer (9.4 GHz) at room temperature with a modulation amplitude of 0.1mT.

Pulse-EPR measurements were carried out at cryogenic temperatures on a home-built W-band spectrometer (95 GHz) equipped with an arbitrary waveform generator (AWG) (Bahrenberg et al., 2017; Goldfarb et al., 2008; Mentink-Vigier et al., 2013). Selecting the observe and pump pulse frequencies is crucial for generating an optimal DEER trace. The echo-detected EPR spectra, along with the setting for nitroxide-nitroxide, Gd(III)-nitroxide, and Gd(III)-Gd(III) DEER measurements are presented in Figure S9 and Table S1.

Echo-detected EPR (ED- EPR) spectra were acquired using the Hahn-Echo pulse sequence (π/2-τ-π-τ-echo) with a two-step phase cycle (0,π) on the first π/2 pulse while keeping τ fixed and sweeping the magnetic field. Echo decays were measured using the same sequence measuring the echo intensity at the maximum of the Gd(III) or the nitroxide signal as a function of τ. The experimental parameters are presented in Table S1

All DEER measurements were performed using the dead-time free four-pulse DEER sequence ($\pi/2_{\nu obs} - \tau_1 - \pi_{\nu obs} - (\tau_1 + t) - \pi_{\nu pump} - (\tau_2 - t) - \pi_{\nu obs} - \tau_2 -$ echo) (Pannier et al., 2000), with a chirp pump pulse generated by the AWG. The echo intensity was measured as a function of t at incremented steps of 20 ns ranging from −200 ns to the set time evolution, $T < \tau_2$. Eight-step phase cycling was used. The experimental parameters are presented in Table S2.

The time-domain DEER traces were analyzed using a Tikhonov regularization-based software package, DeerAnalysis 2019 (Jeschke et al., 2006). The background fitting was carried out assuming a homogenous distribution. The results were validated using the default parameters including the addition of noise.

5.9 | Confocal and fluorescence microscopy

Atto-488 doubly labeled PpiB mutant was delivered into *E. coli* DH5α by EP as described above (see section: "Incorporation into *E. coli* cells") and following earlier reports (Pierro et al., 2022). Once the cells were washed and diluted (1:100, v/v), they were fixed to a 35 mm glass bottom dishes using 4% paraformaldehyde (PFA) (15 min, room temperature). Images were collected using a bright light, confocal, and fluorescence microscope (Leica DMI8 microscope with a ×100/1.4 oil objective) equipped with a 473 nm monochromatic laser.

AUTHOR CONTRIBUTIONS

Yasmin Ben-Ishay: Investigation; writing – original draft; methodology; validation; visualization; writing – review and editing; formal analysis; data curation. **Yoav Barak:** Resources. **Akiva Feintuch:** Investigation. **Olivier Ouari:** Resources. **Annalisa Pierro:** Resources. **Elisabetta Mileo:** Resources. **Xun-Cheng Su:** Resources. **Daniella Goldfarb:** Conceptualization; funding acquisition; writing – original draft; writing – review and editing; methodology; project administration; supervision.

ACKNOWLEDGMENTS

This work was funded by the Joint NSFC (China)-ISF grant (No. 3559/21) and was made possible in part by support from the Helen and Martin Kimmel Institute for Magnetic Resonance Research and the historic generosity of the Harold Perlman Family (D. G.). We also acknowledge financial support from the "Agence Nationale de la Recherche" (ANR-18-CE11-0007-01). Yoav Barak is the incumbent of the Beatrice Barton Research Fellowship.

We gratefully acknowledge Dr. Raanan Carmieli, Dr. Alla Falkovich (Chemical research support), Dr. Yael Fridmann Sirkis, Dr. Inna Goliand, Dr. Tamar Ugner, and Dr. Shira Albeck (Life sciences core facilities) for their assistance to this work. We thank Prof. Gottfried Otting and Dr. Mithun C. Mahawaththa for introducing Yasmin Ben-Ishay to the world of UAA incorporation and spin labeling and Prof. Lital Alfonta, Dr. Inbal Riven, and Prof. Gilad Haran for their assistance in implementing it.

CONFLICT OF INTEREST STATEMENT

The authors declare no conflict of interest.

ORCID

Yasmin Ben-Ishay https://orcid.org/0000-0002-4363-5319

REFERENCES

Abdelkader EH, Feintuch A, Yao X, Adams LA, Aurelio L, Graham B, et al. Protein conformation by EPR spectroscopy using gadolinium tags clicked to genetically encoded p-azido-l-phenylalanine. Chem Commun. 2015;51(88):15898–901. https://doi.org/10.1039/c5cc07121f

Abdelkader EH, Qianzhu H, Tan YJ, Adams LA, Huber T, Otting G. Genetic encoding of N^6-((((trimethylsilyl)methoxy)carbonyl)-L-lysine for NMR studies of protein–protein and protein–ligand interactions. J Am Chem Soc. 2021;143(2):1133–43. https://doi.org/10.1021/jacs.0c11971

Azarkh M, Bieber A, Qi M, Fischer JWA, Yulikov M, Godt A, et al. Gd(III)–Gd(III) relaxation-induced dipolar modulation enhancement for in-cell electron paramagnetic resonance distance determination. J Phys Chem Lett. 2019;10(7):1477–81. https://doi.org/10.1021/acs.jpclett.9b00340

Azarkh M, Okle O, Eyring P, Dietrich DR, Drescher M. Evaluation of spin labels for in-cell EPR by analysis of nitroxide reduction in cell extract of *Xenopus laevis* oocytes. J Magn Reson. 2011;212(2):450–4. https://doi.org/10.1016/j.jmr.2011.07.014

Azarkh M, Okle O, Singh V, Seemann IT, Hartig JS, Dietrich DR, et al. Long-range distance determination in a DNA model system inside *Xenopus laevis* oocytes by in-cell spin-label EPR. Chembiochem. 2011;12(13):1992–5. https://doi.org/10.1002/cbic.201100281

Azarkh M, Singh V, Okle O, Seemann IT, Dietrich DR, Hartig JS, et al. Site-directed spin-labeling of nucleotides and the use of in-cell EPR to determine long-range distances in a biologically relevant environment. Nat Protoc. 2013;8(1):131–47. https://doi.org/10.1038/nprot.2012.136

Bahrenberg T, Rosenski Y, Carmieli R, Zibzener K, Qi M, Frydman V, et al. Improved sensitivity for W-band Gd(III)-Gd(III) and nitroxide-nitroxide DEER measurements with shaped pulses. J Magn Reson. 2017;283:1–13. https://doi.org/10.1016/j.jmr.2017.08.003

Besanceney-Webler C, Jiang H, Zheng T, Feng L, Soriano del Amo D, Wang W, et al. Increasing the efficacy of bioorthogonal click reactions for bioconjugation: a comparative study. Angew Chem Int Ed. 2011;50(35):8051–6. https://doi.org/10.1002/anie.201101817

Bleicken S, Assafa TE, Zhang H, Elsner C, Ritsch I, Pink M, et al. Gem-diethyl pyrroline nitroxide spin labels: synthesis, EPR characterization, rotamer libraries and biocompatibility. ChemistryOpen. 2019;8:1035. https://doi.org/10.1002/open.201900232

Bonucci A, Ouari O, Guigliarelli B, Belle V, Mileo E. In-cell EPR: progress towards structural studies inside cells. Chembiochem. 2020;21(4):451–60. https://doi.org/10.1002/cbic.201900291

Cao C, Chen JL, Yang Y, Huang F, Otting G, Su XC. Selective 15N-labeling of the side-chain amide groups of asparagine and glutamine for applications in paramagnetic NMR spectroscopy. J Biomol NMR. 2014;59(4):251–61. https://doi.org/10.1007/s10858-014-9844-0

Cattani J, Subramaniam V, Drescher M. Room-temperature in-cell EPR spectroscopy: alpha-synuclein disease variants remain intrinsically disordered in the cell. Phys Chem Chem Phys. 2017;19(28):18147–51. https://doi.org/10.1039/c7cp03432f

Cheung MS, Gasic AG. Towards developing principles of protein folding and dynamics in the cell. Phys Biol. 2018;15(6):063001. https://doi.org/10.1088/1478-3975/aaced2

Cohen RD, Pielak GJ. A cell is more than the sum of its (dilute) parts: a brief history of quinary structure. Protein Sci. 2017; 26(3):403–13. https://doi.org/10.1002/pro.3092

Collauto A, von Bülow S, Gophane DB, Saha S, Stelzl LS, Hummer G, et al. Compaction of RNA duplexes in the cell. Angew Chem Int Ed Engl. 2020;59(51):23025–9. https://doi.org/10.1002/anie.202009800

Dalaloyan A, Martorana A, Barak Y, Gataulin D, Reuveny E, Howe A, et al. Tracking conformational changes in calmodulin in vitro, in cell extract, and in cells by electron paramagnetic resonance distance measurements. ChemPhysChem. 2019; 20(14):1860–8. https://doi.org/10.1002/cphc.201900341

Danielsson J, Mu X, Lang L, Wang H, Binolfi A, Theillet FX, et al. Thermodynamics of protein destabilization in live cells. Proc Natl Acad Sci U S A. 2015;112(40):12402–7. https://doi.org/10.1073/pnas.1511308112

Dedmon MM, Patel CN, Young GB, Pielak GJ. FlgM gains structure in living cells. Proc Natl Acad Sci U S A. 2002;99(20):12681–4. https://doi.org/10.1073/pnas.202331299

Dhar A, Girdhar K, Singh D, Gelman H, Ebbinghaus S, Gruebele M. Protein stability and folding kinetics in the nucleus and endoplasmic reticulum of eucaryotic cells. Biophys J. 2011;101(2):421–30. https://doi.org/10.1016/j.bpj.2011.05.071

Ebbinghaus S, Dhar A, McDonald JD, Gruebele M. Protein folding stability and dynamics imaged in a living cell. Nat Methods. 2010;7(4):319–23. https://doi.org/10.1038/nmeth.1435

Edwards KJ, Ollis DL, Dixon NE. Crystal structure of cytoplasmic *Escherichia coli* peptidyl-prolyl isomerase: evidence for decreased mobility of loops upon complexation. J Mol Biol. 1997;271(2):258–65. https://doi.org/10.1006/jmbi.1997.1151

Ellis RJ. Macromolecular crowding: an important but neglected aspect of the intracellular environment. Curr Opin Struct Biol. 2001; 11(1):114–9. https://doi.org/10.1016/S0959-440X(00)00172-X

Fleck N, Heubach CA, Hett T, Haege FR, Bawol PP, Baltruschat H, et al. SLIM: a short-linked, highly redox-stable trityl label for high-sensitivity in-cell EPR distance measurements. Angew Chem Int Ed Engl. 2020;132(24):9854–9. https://doi.org/10.1002/ange.202004452

Freedberg DI, Selenko P. Live cell NMR. Annu Rev Biophys. 2014; 43(1):171–92. https://doi.org/10.1146/annurev-biophys-051013-023136

Galazzo L, Meier G, Januliene D, Parey K, de Vecchis D, Striednig B, et al. The ABC transporter MsbA adopts the wide inward-open conformation in *E. coli* cells. Sci Adv. 2022;8(41): eabn6845. https://doi.org/10.1126/sciadv.abn6845

Garbuio L, Bordignon E, Brooks EK, Hubbell WL, Jeschke G, Yulikov M. Orthogonal spin labeling and Gd(III)-nitroxide distance measurements on bacteriophage T4-lysozyme. J Phys Chem B. 2013;117(11):3145–53. https://doi.org/10.1021/jp401806g

Giannoulis A, Ben-Ishay Y, Goldfarb D. Characteristics of Gd(III) spin labels for the study of protein conformations. In: Cotruvo JA Jr, editor. Methods in Enzymology. Volume 651. 1st ed. Elsevier Inc.; 2021. p. 235–90. https://doi.org/10.1016/bs.mie.2021.01.040

Gnutt D, Timr S, Ahlers J, König B, Manderfeld E, Heyden M, et al. Stability effect of quinary interactions reversed by single point mutations. J Am Chem Soc. 2019;141(11):4660–9. https://doi.org/10.1021/jacs.8b13025

Goldfarb D. Exploring protein conformations in vitro and in cell with EPR distance measurements. Curr Opin Struct Biol. 2022; 75:102398. https://doi.org/10.1016/j.sbi.2022.102398

Goldfarb D, Lipkin Y, Potapov A, Gorodetsky Y, Epel B, Raitsimring AM, et al. HYSCORE and DEER with an upgraded 95 GHz pulse EPR spectrometer. J Magn Reson. 2008;194(1):8–15. https://doi.org/10.1016/j.jmr.2008.05.019

Gruebele M, Pielak GJ. Dynamical spectroscopy and microscopy of proteins in cells. Curr Opin Struct Biol. 2021;70:1–7. https://doi.org/10.1016/j.sbi.2021.02.001

Guignard L, Ozawa K, Pursglove SE, Otting G, Dixon NE. NMR analysis of in vitro-synthesized proteins without purification: a high-throughput approach. FEBS Lett. 2002;524(1–3):159–62. https://doi.org/10.1016/S0014-5793(02)03048-X

Guin D, Gruebele M. Weak chemical interactions that drive protein evolution: crowding, sticking, and quinary structure in folding and function. Chem Rev. 2019;119(18):10691–717. https://doi.org/10.1021/acs.chemrev.8b00753

Guo M, Xu Y, Gruebele M. Temperature dependence of protein folding kinetics in living cells. Proc Natl Acad Sci U S A. 2012; 109(44):17863–7. https://doi.org/10.1073/pnas.1201797109

Guzman I, Gelman H, Tai J, Gruebele M. The extracellular protein VlsE is destabilized inside cells. J Mol Biol. 2014;426(1):11–20. https://doi.org/10.1016/j.jmb.2013.08.024

Hagelueken G, Abdullin D, Ward R, Schiemann O. MtsslSuite: in silico spin labelling, trilateration and distance-constrained rigid body docking in PyMOL. Mol Phys. 2013;111(18–19):2757–66. https://doi.org/10.1080/00268976.2013.809804

Hänsel R, Luh LM, Corbeski I, Trantirek L, Dötsch V. In-cell NMR and EPR spectroscopy of biomacromolecules. Angew Chem Int Ed Engl. 2014;53(39):10300–14. https://doi.org/10.1002/anie.201311320

Heubach CA, Hasanbasri Z, Abdullin D, Reuter A, Korzekwa B, Saxena S, et al. Differentiating between label and protein conformers in pulsed dipolar EPR spectroscopy with the dHis-Cu2+(NTA) motif. Chem A Eur J. 2023;29:e202302541. https://doi.org/10.1002/chem.202302541

Igarashi R, Sakai T, Hara H, Tenno T, Tanaka T, Tochio H, et al. Distance determination in proteins inside *Xenopus laevis* oocytes by double electron-electron resonance experiments. J Am Chem Soc. 2010;132(24):8228–9. https://doi.org/10.1021/ja906104e

Jagtap AP, Krstic I, Kunjir NC, Hänsel R, Prisner TF, Sigurdsson ST. Sterically shielded spin labels for in-cell EPR spectroscopy: analysis of stability in reducing environment. Free Radic Res. 2015;49(1):78–85. https://doi.org/10.3109/10715762.2014.979409

Jana S, Evans EGB, Jang HS, Zhang S, Zhang H, Rajca A, et al. Ultrafast bioorthogonal spin-labeling and distance measurements in mammalian cells using small, genetically encoded tetrazine amino acids. J Am Chem Soc. 2023;145:14608–20. https://doi.org/10.1021/jacs.3c00967

Jash C, Feintuch A, Nudelman S, Manukovsky N, Abdelkader EH, Bhattacharya S, et al. DEER experiments reveal fundamental differences between calmodulin complexes with IQ and MARCKS peptides in solution. Structure. 2022;30(6):813–827. e5. https://doi.org/10.1016/j.str.2022.03.005

Jassoy JJ, Berndh A, Duthie F, Sebastian PK, Hagelueken G, Schiemann O. Versatile trityl spin labels for nanometer

distance measurements on biomolecules in vitro and within cells. Angew Chem Int Ed Engl. 2017;5:177–81. https://doi.org/10.1002/anie.201609085

Jeschke G, Chechik V, Ionita P, Godt A, Zimmermann H, Banham J, et al. DeerAnalysis2006—a comprehensive software package for analyzing pulsed ELDOR data. Appl Magn Reson. 2006;30(3–4):473–98. https://doi.org/10.1007/BF03166213

Jia X, Ozawa K, Loscha K, Otting G. Glutarate and N-acetyl-L-glutamate buffers for cell-free synthesis of selectively 15N-labelled proteins. J Biomol NMR. 2009;44(2):59–67. https://doi.org/10.1007/s10858-009-9315-1

Joseph B, Jaumann EA, Sikora A, Barth K, Prisner TF, Cafiso DS. In situ observation of conformational dynamics and protein ligand–substrate interactions in outer-membrane proteins with DEER/PELDOR spectroscopy. Nat Protoc. 2019;14(8):2344–69. https://doi.org/10.1038/s41596-019-0182-2

Joseph B, Sikora A, Bordignon E, Jeschke G, Cafiso DS, Prisner TF. Distance measurement on an endogenous membrane transporter in *E. coli* cells and native membranes using EPR spectroscopy. Angew Chem Int Ed. 2015;54(21):6196–9. https://doi.org/10.1002/anie.201501086

Karthikeyan G, Bonucci A, Casano G, Gerbaud G, Abel S, Thomé V, et al. A bioresistant Nitroxide spin label for in-cell EPR spectroscopy: in vitro and in oocytes protein structural dynamics studies. Angew Chem Int Ed Engl. 2018;130(5):1380–4. https://doi.org/10.1002/ange.201710184

Klein G, Wojtkiewicz P, Biernacka D, Stupak A, Gorzelak P, Raina S. Identification of substrates of cytoplasmic peptidylprolyl cis/trans isomerases and their collective essentiality in *Escherichia coli*. Int J Mol Sci. 2020;21(12):1–26. https://doi.org/10.3390/ijms21124212

König I, Soranno A, Nettels D, Schuler B. Impact of in-cell and in-vitro crowding on the conformations and dynamics of an intrinsically disordered protein. Angew Chem Int Ed Engl. 2021;60(19):10724–9. https://doi.org/10.1002/anie.202016804

König I, Zarrine-Afsar A, Aznauryan M, Soranno A, Wunderlich B, Dingfelder F, et al. Single-molecule spectroscopy of protein conformational dynamics in live eukaryotic cells. Nat Methods. 2015;12(8):773–9. https://doi.org/10.1038/nmeth.3475

Krstić I, Hänsel R, Romainczyk O, Engels JW, Dötsch V, Prisner TF. Long-range distance measurements on nucleic acids in cells by pulsed EPR spectroscopy. Angew Chem Int Ed Engl. 2011;50(22):5070–4. https://doi.org/10.1002/anie.201100886

Kugele A, Ketter S, Silkenath B, Wittmann V, Joseph B, Drescher M. In situ EPR spectroscopy of a bacterial membrane transporter using an expanded genetic code. Chem Commun. 2021;57(96):12980–3. https://doi.org/10.1039/D1CC04612H

Kwapiszewska K, Kalwarczyk T, Michalska B, Szczepański K, Szymański J, Patalas-Krawczyk P, et al. Determination of oligomerization state of Drp1 protein in living cells at nanomolar concentrations. Sci Rep. 2019;9(1):1–9. https://doi.org/10.1038/s41598-019-42418-0

Liu CC, Schultz PG. Adding new chemistries to the genetic code. Annu Rev Biochem. 2010;79:413–44. https://doi.org/10.1146/annurev.biochem.052308.105824

Loh CT, Ozawa K, Tuck KL, Barlow N, Huber T, Otting G, et al. Lanthanide tags for site-specific ligation to an unnatural amino acid and generation of pseudocontact shifts in proteins. Bioconjug Chem. 2013;24(2):260–8. https://doi.org/10.1021/bc300631z

Luchinat E, Banci L. In-cell NMR: a topical review. IUCrJ. 2017;4:108–18. https://doi.org/10.1107/S2052252516020625

Luchinat E, Banci L. In-cell NMR: from target structure and dynamics to drug screening. Curr Opin Struct Biol. 2022;74:102374. https://doi.org/10.1016/j.sbi.2022.102374

Margineanu A, Chan JJ, Kelly DJ, Warren SC, Flatters D, Kumar S, et al. Screening for protein-protein interactions using Förster resonance energy transfer (FRET) and fluorescence lifetime imaging microscopy (FLIM). Sci Rep. 2016;6. https://doi.org/10.1038/srep28186

Martorana A, Bellapadrona G, Feintuch A, Di Gregorio E, Aime S, Goldfarb D. Probing protein conformation in cells by EPR distance measurements using Gd3+ spin labeling. J Am Chem Soc. 2014;136(38):13458–65. https://doi.org/10.1021/ja5079392

McConkey EH. Molecular evolution, intracellular organization, and the quinary structure of proteins. Proc Natl Acad Sci U S A. 1982;79(10):3236–40. https://doi.org/10.1073/pnas.79.10.3236

McGuffee SR, Elcock AH. Diffusion, crowding & protein stability in a dynamic molecular model of the bacterial cytoplasm. PLoS Comput Biol. 2010;6(3):e1000694. https://doi.org/10.1371/journal.pcbi.1000694

Mentink-Vigier F, Collauto A, Feintuch A, Kaminker I, Tarle V, Goldfarb D. Increasing sensitivity of pulse EPR experiments using echo train detection schemes. J Magn Reson. 2013;236:117–25. https://doi.org/10.1016/j.jmr.2013.08.012

Milles S, Tyagi S, Banterle N, Koehler C, VanDelinder V, Plass T, et al. Click strategies for single-molecule protein fluorescence. J Am Chem Soc. 2012;134(11):5187–95. https://doi.org/10.1021/ja210587q

Monteitha WB, Pielak GJ. Residue level quantification of protein stability in living cells. Proc Natl Acad Sci U S A. 2014;111(31):11335–40. https://doi.org/10.1073/pnas.1406845111

Orton HW, Qianzhu H, Abdelkader EH, Habel EI, Tan YJ, Frkic RL, et al. Through-space scalar 19F-19F couplings between fluorinated noncanonical amino acids for the detection of specific contacts in proteins. J Am Chem Soc. 2021;143(46):19587–98. https://doi.org/10.1021/jacs.1c10104

Ozawa K, Dixon N, Otting G. Cell-free synthesis of 15 N-labeled proteins for NMR studies. IUBMB Life. 2005;57(9):615–22. https://doi.org/10.1080/15216540500217859

Ozawa K, Headlam MJ, Mouradov D, Watt SJ, Beck JL, Rodgers KJ, et al. Translational incorporation of L-3,4-dihydroxyphenylalanine into proteins. FEBS J. 2005;272(12):3162–71. https://doi.org/10.1111/j.1742-4658.2005.04735.x

Ozawa K, Headlam MJ, Schaeffer PM, Henderson BR, Dixon NE, Otting G. Optimization of an *Escherichia coli* system for cell-free synthesis of selectively 15N-labelled proteins for rapid analysis by NMR spectroscopy. Eur J Biochem. 2004;271(20):4084–93. https://doi.org/10.1111/j.1432-1033.2004.04346.x

Pannier M, Veit S, Godt A, Jeschke G, Spiess HW. Dead-time free measurement of dipole–dipole interactions between electron spins. J Magn Reson. 2000;142(2):331–40. https://doi.org/10.1006/jmre.1999.1944

Phillip Y, Kiss V, Schreiber G. Protein-binding dynamics imaged in a living cell. Proc Natl Acad Sci U S A. 2012;109(5):1461–6. https://doi.org/10.1073/pnas.1112171109

Pierro A, Bonucci A, Normanno D, Ansaldi M, Pilet E, Ouari O, et al. Probing the structural dynamics of a bacterial chaperone in its native environment by nitroxide-based EPR spectroscopy. Chem A Eur J. 2022;28:e202202249. https://doi.org/10.1002/chem.202202249

Plitzko JM, Schuler B, Selenko P. Structural biology outside the box—inside the cell. Curr Opin Struct Biol. 2017;46:110–21. https://doi.org/10.1016/j.sbi.2017.06.007

Qi M, Groß A, Jeschke G, Godt A, Drescher M. Gd(III)-PyMTA label is suitable for in-cell EPR. J Am Chem Soc. 2014;136(43):15366–78. https://doi.org/10.1021/ja508274d

Qianzhu H, Welegedara AP, Williamson H, McGrath AE, Mahawaththa MC, Dixon NE, et al. Genetic encoding of para-pentafluorosulfanyl phenylalanine: a highly hydrophobic and strongly electronegative group for stable protein interactions. J Am Chem Soc. 2020;142(41):17277–81. https://doi.org/10.1021/jacs.0c07976

Qin S, Zhou H-X. Protein folding, binding, and droplet formation in cell-like conditions. Curr Opin Struct Biol. 2017;43(1):28–37. https://doi.org/10.1016/j.sbi.2016.10.006

Rivas G, Minton AP. Macromolecular crowding in vitro, in vivo, and in between. Trends Biochem Sci. 2016;41(11):970–81. https://doi.org/10.1016/j.tibs.2016.08.013

Rivas G, Minton AP. Toward an understanding of biochemical equilibria within living cells. Biophys Rev. 2018;10(2):241–53. https://doi.org/10.1007/s12551-017-0347-6

Schägger H. Tricine-SDS-PAGE. Nat Protoc. 2006;1(1):16–22. https://doi.org/10.1038/nprot.2006.4

Schlesinger AP, Wang Y, Tadeo X, Millet O, Pielak GJ. Macromolecular crowding fails to fold a globular protein in cells. J Am Chem Soc. 2011;133(21):8082–5. https://doi.org/10.1021/ja201206t

Schmidt MJ, Borbas J, Drescher M, Summerer D. A genetically encoded spin label for electron paramagnetic resonance distance measurements. J Am Chem Soc. 2014;136(4):1238–41. https://doi.org/10.1021/ja411535q

Shenberger Y, Gevorkyan Aiapetov L, Hirsch M, Hofmann L, Ruthstein S. An in-cell spin-labelling methodology provides structural information on cytoplasmic proteins in bacteria. Chem Commun. 2023;59:10524–7. https://doi.org/10.1039/D3CC03047D

Singewald K, Lawless MJ, Saxena S. Increasing nitroxide lifetime in cells to enable in-cell protein structure and dynamics measurements by electron spin resonance spectroscopy. J Magn Reson. 2019;299:21–7. https://doi.org/10.1016/j.jmr.2018.12.005

Skagia A, Zografou C, Vezyri E, Venieraki A, Katinakis P, Dimou M. Cyclophilin PpiB is involved in motility and biofilm formation via its functional association with certain proteins. Genes Cells. 2016;21(8):833–51. https://doi.org/10.1111/gtc.12383

Su XC, Loh CT, Qi R, Otting G. Suppression of isotope scrambling in cell-free protein synthesis by broadband inhibition of PLP enymes for selective 15N-labelling and production of perdeuterated proteins in H_2O. J Biomol NMR. 2011;50(1):35–42. https://doi.org/10.1007/s10858-011-9477-5

Sukenik S, Ren P, Gruebele M. Weak protein-protein interactions in live cells are quantified by cell-volume modulation. Proc Natl Acad Sci U S A. 2017;114(26):6776–81. https://doi.org/10.1073/pnas.1700818114

Takeda M, Jee J, Ono AM, Terauchi T, Kainosho M. Hydrogen exchange study on the hydroxyl groups of serine and threonine residues in proteins and structure refinement using NOE restraints with polar side-chain groups. J Am Chem Soc. 2011;133(43):17420–7. https://doi.org/10.1021/ja206799v

Theillet FX. In-cell structural biology by NMR: the benefits of the atomic scale. Chem Rev. 2022;122(10):9497–570. https://doi.org/10.1021/acs.chemrev.1c00937

Theillet FX, Binolfi A, Bekei B, Martorana A, Rose HM, Stuiver M, et al. Structural disorder of monomeric α-synuclein persists in mammalian cells. Nature. 2016;530(7588):45–50. https://doi.org/10.1038/nature16531

Torricella F, Bonucci A, Polykretis P, Cencetti F, Banci L. Rapid protein delivery to living cells for biomolecular investigation. Biochem Biophys Res Commun. 2021;570:82–8. https://doi.org/10.1016/j.bbrc.2021.07.006

Tyagi S, Lemke EA. Genetically encoded click chemistry for single-molecule FRET of proteins. In: Conn PM, editor. Laboratory methods in cell biology. Volume 113. Elsevier Inc.; 2013. p. 169–87. https://doi.org/10.1016/B978-0-12-407239-8.00009-4

Wang M, Song X, Chen J, Chen X, Zhang X, Yang Y, et al. Intracellular environment can change protein conformational dynamics in cells through weak interactions. Sci Adv. 2023;9(29):1–10. https://doi.org/10.1126/sciadv.adg9141

Wang X-W, Zhang X, Cui C-Y, Li B, Goldfarb D, Yang Y, et al. Stabilizing nitroxide spin labels for structural and conformational studies of biomolecules by maleimide treatment. Chem A Eur J. 2023;29:e202301350. https://doi.org/10.1002/chem.202301350

Wang Y, Sarkar M, Smith AE, Krois AS, Pielak GJ. Macromolecular crowding and protein stability. J Am Chem Soc. 2012;134(40):16614–8. https://doi.org/10.1021/ja305300m

Wang Y-S, Fang X, Wallace AL, Wu B, Liu WR. A rationally designed pyrrolysyl-tRNA synthetase mutant with a broad substrate spectrum. J Am Chem Soc. 2012;134(6):2950–3. https://doi.org/10.1021/ja211972x

Welegedara AP, Adams LA, Huber T, Graham B, Otting G. Site-specific incorporation of selenocysteine by genetic encoding as a photocaged unnatural amino acid. Bioconjug Chem. 2018;29(7):2257–64. https://doi.org/10.1021/acs.bioconjchem.8b00254

Widder P, Schuck J, Summerer D, Drescher M. Combining site-directed spin labeling: in vivo and in-cell EPR distance determination. Phys Chem Phys. 2020;22(9):4875–9. https://doi.org/10.1039/c9cp05584c

Wu PSC, Ozawa K, Lim SP, Vasudevan SG, Dixon NE, Otting G. Cell-free transcription/translation from PCR-amplified DNA for high-throughput NMR studies. Angew Chem Int Ed Engl. 2007;46(18):3356–8. https://doi.org/10.1002/anie.200605237

Yang Y, Chen S-N, Yang F, Li X-Y, Feintuch A, Su X-C, et al. In-cell destabilization of a homodimeric protein complex detected by DEER spectroscopy. Proc Natl Acad Sci U S A. 2020;117(34):20566–75. https://doi.org/10.1073/pnas.2005779117

Yang Y, Pan BB, Tan X, Yang F, Liu Y, Su XC, et al. In-cell trityl-trityl distance measurements on proteins. J Phys Chem Lett. 2020;11(3):1141–7. https://doi.org/10.1021/acs.jpclett.9b03208

Yang Y, Yang F, Gong YJ, Bahrenberg T, Feintuch A, Su XC, et al. High sensitivity in-cell EPR distance measurements on proteins using an optimized Gd(III) spin label. J Phys Chem Lett. 2018;9(20):6119–23. https://doi.org/10.1021/acs.jpclett.8b02663

Yang Y, Yang F, Gong YJ, Chen JL, Goldfarb D, Su XC. A reactive, rigid GdIII labeling tag for in-cell EPR distance measurements in proteins. Angew Chem Int Ed Engl. 2017;56(11):2914–8. https://doi.org/10.1002/anie.201611051

Yang Y, Yang F, Li XY, Su XC, Goldfarb D. In-cell EPR distance measurements on ubiquitin labeled with a rigid PyMTA-Gd(III) tag. J Phys Chem B. 2019;123(5):1050–9. https://doi.org/10.1021/acs.jpcb.8b11442

Yu I, Mori T, Ando T, Harada R, Jung J, Sugita Y, et al. Biomolecular interactions modulate macromolecular structure and dynamics in atomistic model of a bacterial cytoplasm. Elife. 2016;5:1–22. https://doi.org/10.7554/eLife.19274

Zhou HX, Rivas G, Minton AP. Macromolecular crowding and confinement: biochemical, biophysical, and potential physiological consequences. Annu Rev Biophys. 2008;37:375–97. https://doi.org/10.1146/annurev.biophys.37.032807.125817

SUPPORTING INFORMATION

Additional supporting information can be found online in the Supporting Information section at the end of this article.

How to cite this article: Ben-Ishay Y, Barak Y, Feintuch A, Ouari O, Pierro A, Mileo E, et al. Exploring the dynamics and structure of PpiB in living *Escherichia coli* cells using electron paramagnetic resonance spectroscopy. Protein Science. 2024;33(3):e4903. https://doi.org/10.1002/pro.4903